Chapter 8

BIT for Free Surface Flows

G. Baker

Department of Mathematics,
The Ohio State University,
231 W. 18th Ave, Columbus OH 43210,
USA
baker@math.ohio-state.edu

Boundary integral techniques (BIT) offer several advantages for tracking free surfaces in inviscid fluids. They reduce the spatial dimension by one in that only information on the surface is needed to advance the location of the surface. For irrotational flow, the fluid velocity is given by the gradient of a velocity potential which satisfies Laplace's equation. Formal solutions can be expressed in terms of Green's functions for Laplace's equation and these solutions lead to elegant formulations for free surface flows. In particular, dipole distributions along the surface provide a perfect representation for the potential since the normal derivatives are continuous across the surface, one of the required boundary conditions. Lagrangian markers on the surface move with a weighted average of the fluid velocities, the weighting based on the difference in densities across the surface. This choice provides a natural adaption in the representation of the surface in time. Finally, Bernoulli's equation can be used to satisfy the dynamic boundary condition at the surface, leading to an integral equation for the dipole strength. This formulation, provided in this chapter, has been used successfully in the study of water waves, the Rayleigh-Taylor instability and the rise of bubbles. Modifications are presented for the case of multiple surfaces and the presence of solid boundaries.

8.1. The Nature of Free Surface Flows

Free surfaces abound everywhere. The most common example is the interface between water and air. We see these surfaces as rain drops, ocean waves, a glass of water, etc. They appear over a vast range of length scales

and they encompass multiple phenomena: jets of water that break into drops, waves that crash on the shore; mixtures of oil and water in porous rock (oil reservoirs); rivulets of water flowing down a window pane. The list goes on and on. The fascination we find in water surfaces has naturally attracted scientists to develop mathematical models to describe their behaviour. By far, the most common studies assume continuum models with a sharp interface. In particular, the Euler equations or the Navier-Stokes equations are used for the fluid flow and jump conditions that satisfy kinematic and dynamic conditions are imposed at the surface. These models have been thoroughly tested over the last few centuries, and they are now well accepted as good models for free surface flow.

Despite the great success of the standard models for free surface flow, there remain aspects of their behaviour far less well understood, in particular when free surfaces undergo topological changes as in the break-up of a liquid jet into droplets. The separation of a droplet from the jet happens almost instantaneously on a molecular level that makes it extraordinarily difficult to express in a mathematical model, especially one that is a continuum model. Further difficulties in mathematical models arise at the point of contact between a free surface and a solid boundary, the so-called contact-line problem. These difficulties will not be addressed here.

Even when the surface remains smooth without topological changes, the full equations of motion are nonlinear and must be solved in a changing geometry. Not surprisingly, many studies of free surface flow have employed various approximations of the basic equations or restricted the nature of the free surface in some way to make the mathematical problems tractable. A vast body of knowledge has been gained this way and has served the scientific community well. Over the last century, with the advent of high-speed computing, several numerical methods have been developed to track free surface motion. Some of the popular ones include level set methodology, front-tracking techniques and finite volume methods. The overriding factor that emerges from these approaches is the importance of highly accurate calculations of the free surface velocities. Otherwise, the numerical evolution of the surface quickly becomes inaccurate and can lead to unphysical behaviour. The challenge, then, is the continual improvement of numerical techniques that ensure accurate and reliable calculations of free surface flow.

There are two classes of free surface flows where boundary integrals have a natural advantage over other methods. They are characterized by very large or very small Reynolds numbers. The Reynolds number is the ratio

of inertial forces to viscous forces. It is small when viscous effects dominate, such as the motion of small drops; it is large when viscous effects are negligible, such as the propagation of water waves. In the former case, the fluid equations can be reduced to the solution of a bi-harmonic equation: this topic is covered thoroughly by Pozrikidis.[1] In the latter case, the fluid equations can be reduced to the solution of Laplace's equation. Here, it is natural to use source or dipole distributions along the surface, and the velocity at the surface can be expressed completely by boundary integrals of these distributions. In essence, only information on the surface is needed to update the surface, thus reducing the effective spatial dimension of the problem by one. Further, the surface may be represented explicitly through a surface parametrization; there is no need to embed the surface in a numerical grid.

In the next section, boundary integrals will be formulated as the solution to Euler's equation of fluid motion with free surfaces. The formulation is for a surface between two fluids of constant but different densities in three-dimensional flow. The restriction to two-dimensional flow is included separately to illustrate its connection to complex analysis, a powerful tool that allows improved numerical methods. The challenge for numerical simulations is reliable and accurate calculation of the boundary integrals which contain singular integrands. This issue is addressed in Section 8.3. In particular, there are some highly accurate methods for surfaces (curves) in two-dimensional flow. These methods are applied to several free surface flow problems in Section 8.4 which contain a single free surface, such as water waves, Rayleigh-Taylor instabilities and rising bubbles. The extension to more free surfaces is straightforward, but an additional boundary integral formulation is needed when solid boundaries are present (described in Section 8.5). Yet, there remain difficulties and the chapter will close in describing some of them.

8.2. Mathematical Formulation

Euler's equations for fluid flow in the absence of viscous effects are:

$$\frac{\partial \rho}{\partial t} + (\mathbf{u} \cdot \nabla)\rho = 0\,, \tag{8.1}$$

$$\frac{\partial \mathbf{u}}{\partial t} + (\mathbf{u} \cdot \nabla)\mathbf{u} = -\frac{1}{\rho}\nabla p + \mathbf{g}\,, \tag{8.2}$$

where $\mathbf{u}$ is the fluid velocity, ρ is the density, p is the hydrodynamic pressure and $\rho\mathbf{g}$ is the gravitational force. For liquids and gases moving slowly, it is

usual to assume the flow is incompressible,

$$\nabla \cdot \mathbf{u} = 0\,. \tag{8.3}$$

Equations (8.1 – 8.2) are evolution equations for ρ and $\mathbf{u}$, with Eq. (8.3) acting as a constraint that determines p.

Another form of these equations uses the vorticity $\boldsymbol{\omega} = \nabla \times \mathbf{u}$. By taking the curl of Eq. (8.2), an evolution equation for the vorticity is derived.

$$\frac{\partial \boldsymbol{\omega}}{\partial t} + (\mathbf{u} \cdot \nabla)\boldsymbol{\omega} - (\boldsymbol{\omega} \cdot \nabla)\mathbf{u} = \nabla p \times \nabla \left(\frac{1}{\rho}\right)\,. \tag{8.4}$$

Now the velocity must be determined from Eq. (8.3) and the definition of the vorticity. A standard approach is to introduce the vector potential $\mathbf{A}$ by $\mathbf{u} = \nabla \times \mathbf{A}$. This choice automatically satisfies Eq. (8.3), and the definition of the vorticity becomes

$$\nabla^2 \mathbf{A} = -\boldsymbol{\omega}\ , \tag{8.5}$$

with the additional requirement $\nabla \cdot \mathbf{A} = 0$. Several books[2–4] provide excellent coverage of vorticity and vortex methods, which have direct connections to the methods described in this chapter.

A particular value of the vorticity formulation Eq. (8.4) is that it draws attention to the production of vorticity. The terms on the left-hand side of Eq. (8.4) describe the advection and stretching of vortex lines, and the term on the right-hand side describes how vorticity may be created. In the absence of solid boundaries, vorticity can only be produced from density gradients. For flows where it is reasonable to assume density is uniform, vorticity is conserved. In particular, if there is no initial vorticity, then there will be none in the future.

On the other hand, if there is a sharp interface separating regions of constant but different densities, then vorticity is created at the interface. Unfortunately, the production of vorticity on the interface is a generalized function and difficult to derive from Eq. (8.4) directly. Instead, it is easier to seek solutions in each region separately and then connect them through interfacial conditions at the surface.

In each region, the velocity must be curl-free. Consequently, the velocity may be expressed in terms of a velocity potential $\mathbf{u} = \nabla\phi$. Upon substitution into Eq. (8.2), the equation may be integrated to produce Bernoulli's equation,

$$\frac{\partial \phi}{\partial t} + \frac{1}{2}(\nabla\phi)^2 + \frac{p}{\rho} + gy = C(t)\,, \tag{8.6}$$

where it is now assumed that y is a coordinate in the upward vertical direction. Further, Eq. (8.3) becomes

$$\nabla^2\phi = 0\,. \tag{8.7}$$

The way forward is to use Bernoulli's equation, Eq. (8.6), to update the potential at the surface, and then to use the result as a Dirichlet boundary condition for the solution to Laplace's equation, Eq. (8.7). This is where boundary integral techniques come into play.

8.2.1. *Three-dimensional BIT*

Quite clearly, Eq. (8.5) and Eq. (8.7) are candidates for boundary integral methods. To proceed, boundary conditions are needed. Consider a sharp interface between two immiscible fluids of different densities. The interface must move with the fluid: this requires that the normal component of the fluid velocities at the interface match the normal velocity of the interface. Let $\mathbf{n}$ be the unit normal to the surface pointing outwards if the surface is closed and pointing downward if the surface is open and extends to infinity in the horizontal direction. Designate the fluid quantities on either side of the interface by the subscript 1 if the quantity is on the outside (below) the surface and subscript 2 if it is inside (above). Then the kinematic condition is that the normal components of the fluid velocities must match:

$$\mathbf{n}\cdot\mathbf{u}_1 = \mathbf{n}\cdot\mathbf{u}_2\,. \tag{8.8}$$

Dynamic considerations require that the pressure jump across the interface is balanced by the interfacial force due to surface tension.

$$p_2 - p_1 = T\kappa\,. \tag{8.9}$$

The surface tension coefficient is T and the curvature is κ. Boundary integrals are needed that satisfy Eqs (8.8 – 8.9).

There are many choices for boundary integrals that solve elliptic problems. One in particular offers advantages for free surface flows. Dipole distributions automatically guarantee continuity of the normal derivatives of the potential, in other words, continuity of the normal components of velocity Eq. (8.8). Let μ be a dipole strength distributed along the interface written in parametric form as $\mathbf{x}(\mathbf{p},t)$, where $\mathbf{p}$ represents two surface coordinates (p_1,p_2).[a] Then the potential generated by the dipole distribution

[a]The dependency on time will no longer be explicitly indicated unless necessary.

along the surface is

$$\phi(\mathbf{x}) = \int \mu(\mathbf{q})\, \mathbf{n}(\mathbf{q}) \cdot \nabla_q G\big(\mathbf{x} - \mathbf{x}(\mathbf{q})\big)\, \mathrm{d}S(\mathbf{q})\,. \tag{8.10}$$

The subscript q on ∇ indicates that the gradient is with respect to $\mathbf{x}(\mathbf{q})$, i.e. the second argument of G. The Green's function G depends on the dimensions of the elliptic equation. In two dimensions,

$$G(\mathbf{x} - \mathbf{x}(\mathbf{q})) = \frac{1}{2\pi} \ln\big|\mathbf{x} - \mathbf{x}(\mathbf{q})\big|\,, \tag{8.11}$$

and in three dimensions,

$$G(\mathbf{x} - \mathbf{x}(\mathbf{q})) = -\frac{1}{4\pi}\, \frac{1}{\big|\mathbf{x} - \mathbf{x}(\mathbf{q})\big|}\,. \tag{8.12}$$

While the normal derivative of the potential is continuous across the interface, the potential jumps in value by μ. Specifically, as $\mathbf{x} \to \mathbf{x}(\mathbf{p})$ approaches the interface along the normal direction, the potential has the limiting values,[b]

$$\phi_1(\mathbf{p}) = I(\mathbf{p}) - \frac{\mu(\mathbf{p})}{2}\,, \tag{8.13}$$

$$\phi_2(\mathbf{p}) = I(\mathbf{p}) + \frac{\mu(\mathbf{p})}{2}\,, \tag{8.14}$$

where

$$I(\mathbf{p}) = \int \mu(\mathbf{q})\, \mathbf{n}(\mathbf{q}) \cdot \nabla_q G\big(\mathbf{x}(\mathbf{p}) - \mathbf{x}(\mathbf{q})\big)\, \mathrm{d}S(\mathbf{q})\,. \tag{8.15}$$

This integral must be interpreted as a principal-valued integral. It gives the average value of the potentials on either side of the interface, and the dipole strength is the jump in value of the potential across the interface. These statements follow by simply adding or subtracting Eq. (8.13) and Eq. (8.14).

So far, the potential ϕ generated by Eq. (8.10) satisfies Eq. (8.7) and the interfacial condition Eq. (8.8). The other interfacial condition Eq. (8.9) will determine μ. Before describing how, let's determine first how the velocity of the interface can be calculated when μ is considered known. The first issue to face is the choice for the velocity of the interface. While the normal component is continuous, the tangential components may jump. A flexible choice is to take a weighted average,

$$\frac{\partial \mathbf{x}}{\partial t} = \mathbf{u}_I \equiv \frac{1}{2}\big[(1+\alpha)\mathbf{u}_1 + (1-\alpha)\mathbf{u}_2\big]\,, \tag{8.16}$$

[b]The limiting behaviour depends on the choice of direction of the normal in Eq. (8.10), so the sign of the jump in the potential may be different from other derivations.

where the parameter α controls the weighting. For example, when $\alpha = 1$, the velocity of the interface is the velocity of the outer (lower) fluid. The time derivative of the location of the interface is written with partial derivatives to emphasize that the surface location $\mathbf{p}$ is held fixed. In other words, the motion of the interface is Lagrangian and $\mathbf{p}$ represents the Lagrangian label.

In line with the nature of the potential at the surface, define the average velocity and the jump in velocity as

$$\mathbf{U} = \frac{1}{2}\big(\mathbf{u}_1 + \mathbf{u}_2\big)\,, \quad \mathbf{m} = \mathbf{u}_2 - \mathbf{u}_1\,. \tag{8.17}$$

Consequently, the interfacial velocity is

$$\mathbf{u}_I = \mathbf{U} - \frac{\alpha}{2}\,\mathbf{m}\,. \tag{8.18}$$

The goal now is to determine $\mathbf{U}$ and $\mathbf{m}$ by using information on the surface only.

The tangential velocity components can be determined directly from the tangential derivatives of the potential evaluated along the surface. Specifically, let $\phi(p_1, p_2) = \phi\big(\mathbf{x}(\mathbf{p})\big)$ represent either the potential above or below evaluated on the surface and differentiate with respect to p_1 and p_2 separately.

$$\frac{\partial \phi}{\partial p_1} = \frac{\partial \mathbf{x}}{\partial p_1} \cdot \nabla \phi\,, \quad \text{and} \quad \frac{\partial \phi}{\partial p_2} = \frac{\partial \mathbf{x}}{\partial p_2} \cdot \nabla \phi\,. \tag{8.19}$$

Since

$$\mathbf{t}_1 = \frac{\partial \mathbf{x}}{\partial p_1}\,, \quad \mathbf{t}_2 = \frac{\partial \mathbf{x}}{\partial p_2}\,, \tag{8.20}$$

are tangent vectors (not necessarily unit vectors), the tangential components of the velocities at the interface give

$$\mathbf{t}_1 \cdot \mathbf{U} = \frac{\partial I}{\partial p_1}\,, \quad \mathbf{t}_2 \cdot \mathbf{U} = \frac{\partial I}{\partial p_2}\,, \tag{8.21}$$

$$\mathbf{t}_1 \cdot \mathbf{m} = \frac{\partial \mu}{\partial p_1}\,, \quad \mathbf{t}_2 \cdot \mathbf{m} = \frac{\partial \mu}{\partial p_2}\,. \tag{8.22}$$

The tangent vectors may be used to determine the unit normal to the interface,

$$\big|\mathbf{t}_1 \times \mathbf{t}_2\big|\,\mathbf{n} = \mathbf{t}_1 \times \mathbf{t}_2\,. \tag{8.23}$$

The assumption is that the orientation of the tangent vectors are such as to make the normal vector point outwards (below). The next step is to find a

way to determine the normal velocity component $\mathbf{n}\cdot\nabla\phi$. One way forward is to use Green's theorem to formulate a boundary integral equation for the normal derivative of ϕ, given ϕ on the surface. This approach is often used when either ρ_1 or ρ_2 is zero, but it may be possible to use it in the general case.

An alternative approach is based on tangential derivatives of the vector potential. Fortunately, the vector potential can be determined by a boundary integral of the dipole distribution. Start with $\nabla\phi = \nabla\times\mathbf{A}$, and use the vector identity,

$$\begin{aligned}\nabla_p\Big(\mathbf{n}(q)\cdot\nabla_q G\big(\mathbf{x}(\mathbf{p})-\mathbf{x}(\mathbf{q})\big)\Big) &= \Big(\mathbf{n}(q)\cdot\nabla_p\Big)\Big(\nabla_q G\big(\mathbf{x}(\mathbf{p})-\mathbf{x}(\mathbf{q})\big)\Big)\\ &= -\nabla_p\times\Big(\mathbf{n}(q)\times\nabla_q G\big(\mathbf{x}(\mathbf{p})-\mathbf{x}(\mathbf{q})\big)\Big)\,,\end{aligned}$$

to derive the expression for the vector potential,

$$\mathbf{A}(\mathbf{p}) = -\int \mu(\mathbf{q})\,\mathbf{n}(\mathbf{q})\times\nabla_q G\big(\mathbf{x}(\mathbf{p})-\mathbf{x}(\mathbf{q})\big)\,\mathrm{d}S(\mathbf{q})\,, \tag{8.24}$$

where

$$\mathrm{d}S(q) = \big|\mathbf{t}_1\times\mathbf{t}_2\big|\,\mathrm{d}p_1\,\mathrm{d}p_2\,.$$

The vector potential is continuous across the interface so its tangential derivatives do not jump in value. Apply the identity

$$\iint \nabla\times\mathbf{A}\cdot\mathbf{n}\,\mathrm{d}S = \int \mathbf{A}\cdot\mathrm{d}\mathbf{l} \tag{8.25}$$

to a small closed region lying on the interface. The result gives

$$\big(\mathbf{t}_1\times\mathbf{t}_2\big)\cdot\mathbf{U} = \frac{\partial A_2}{\partial p_1} - \frac{\partial A_1}{\partial p_2}\,, \tag{8.26}$$

where

$$A_1 = \mathbf{t}_1\cdot\mathbf{A}\,,\quad A_2 = \mathbf{t}_2\cdot\mathbf{A}\,. \tag{8.27}$$

The quantities A_1 and A_2 are integrals that result from applying the dot product to Eq. (8.24).

Equations (8.20 – 8.21, and 8.26) determine the velocity at the interface. They constitute a set of linear equations for $\mathbf{U}$ and $\mathbf{m}$ which may be solved in closed form to give

$$|\mathbf{t}_1\times\mathbf{t}_2|\,\mathbf{U} = \mathbf{t}_2\times\mathbf{n}\,\frac{\partial I}{\partial p_1} - \mathbf{t}_1\times\mathbf{n}\,\frac{\partial I}{\partial p_2} + \mathbf{n}\left[\frac{\partial A_2}{\partial p_1} - \frac{\partial A_1}{\partial p_2}\right], \tag{8.28}$$

$$|\mathbf{t}_1\times\mathbf{t}_2|\,\mathbf{m} = \mathbf{t}_2\times\mathbf{n}\,\frac{\partial \mu}{\partial p_1} - \mathbf{t}_1\times\mathbf{n}\,\frac{\partial \mu}{\partial p_2}\,. \tag{8.29}$$

The result shows that $\mathbf{U}$ can be determined by the surface derivatives of three boundary integrals, I Eq. (8.15) and A_1 and A_2 Eq. (8.27) . The two results, Eqs (8.28 – 8.29), determine $\mathbf{u}_I$ Eq. (8.15) which completes the specification of the velocity of a Lagrangian marker on the interface Eq. (8.16). So far, no information other than surface quantities need to be known.

The last step is the derivation of an evolution equation for the dipole strength. This derivation must use Bernoulli's equation Eq. (8.6) and the dynamic boundary condition Eq. (8.9), but Bernoulli's equation must be transformed to account for the Lagrangian motion of the surface markers (fixed $\mathbf{p}$). The change in potential following the Lagrangian motion on either side of the interface is

$$\rho_1 \left[\frac{\partial \phi_1}{\partial t} - \mathbf{u}_I \cdot \mathbf{u}_1 + \frac{1}{2} |\mathbf{u}_1|^2 + gy \right] + p_1 = 0 \,, \tag{8.30}$$

$$\rho_2 \left[\frac{\partial \phi_2}{\partial t} - \mathbf{u}_I \cdot \mathbf{u}_2 + \frac{1}{2} |\mathbf{u}_2|^2 + gy \right] + p_2 = 0 \,. \tag{8.31}$$

By subtracting Eq. (8.31) from Eq. (8.30) and using the definitions of the surface velocity Eq. (8.18), one finds after some lengthy algebra,

$$\frac{1}{2} \frac{\partial \mu}{\partial t} - A \frac{\partial I}{\partial t} = -\frac{\alpha}{4} |\mathbf{m}|^2 - A \left[\frac{1}{2} |\mathbf{U}|^2 - \frac{\alpha}{2} \mathbf{m} \cdot \mathbf{U} - \frac{1}{8} |\mathbf{m}|^2 - gy \right] - \frac{T}{\rho_1 + \rho_2} \kappa \,. \tag{8.32}$$

The Atwood number measures the jump in the density and is defined as

$$A = \frac{\rho_1 - \rho_2}{\rho_1 + \rho_2} \,. \tag{8.33}$$

The time derivative of I can be split into two parts:

$$\frac{\partial I}{\partial t} = \int \frac{\partial \mu(\mathbf{q})}{\partial t} \, \mathbf{n}(\mathbf{q}) \cdot \nabla_q G\big(\mathbf{x}(\mathbf{p}) - \mathbf{x}(\mathbf{q})\big) \, \big|\mathbf{t}_1 \times \mathbf{t}_2\big| \, \mathrm{d}p_1 \, \mathrm{d}p_2 + \int \mu(\mathbf{q}) \, \frac{\partial}{\partial t} \Big\{ \mathbf{n}(\mathbf{q}) \cdot \nabla_q G\big(\mathbf{x}(\mathbf{p}) - \mathbf{x}(\mathbf{q})\big) \, \big|\mathbf{t}_1 \times \mathbf{t}_2\big| \Big\} \, \mathrm{d}p_1 \, \mathrm{d}p_2 \,. \tag{8.34}$$

The time derivative in the second integral must be taken carefully since all the quantities in the braces depend on time through their dependency on $\mathbf{x}(\mathbf{p}, t)$. The time derivative of $\mathbf{x}(\mathbf{p}, t)$ is $\mathbf{u}_I$ which depends only on μ and the location of the interface and may be calculated as already described above. Consequently, the second integral and the right-hand side of Eq. (8.32) may be calculated provided only that μ is known. The first integral in Eq. (8.34)

coupled with the first term in Eq. (8.32) forms a Fredholm integral equation of the second kind for the rate of change of the dipole strength, and its solution provides a way to update μ.

In summary, Eqs (8.16, 8.18, 8.28, 8.29 and 8.32) constitute a set of evolution equations for $\mathbf{x}$ and μ. Knowing $\mathbf{x}$ and μ at some time t, the tangent vectors Eq. (8.20) and the normal Eq. (8.23) may be evaluated, and then the boundary integrals Eqs (8.15 and 8.27) may be evaluated to determine the average velocity $\mathbf{U}$ and the velocity difference $\mathbf{m}$ from Eqs (8.28 and 8.29). This gives the interfacial velocity $\mathbf{u}_I$ defined in Eq. (8.18). Finally, the right-hand side terms of Eq. (8.32) may be evaluated, including the second integral in Eq. (8.34), and the integral equation Eq. (8.32) may be solved to obtain the rate of change of the dipole strength. Consequently, the surface location and the dipole strength may be updated in time.

The dipole strength has a direct connection to a special distribution of vorticity on the interface. By integrating by parts, Eq. (8.24) may be written as

$$\mathbf{A} = -\int \boldsymbol{\omega}\,(\mathbf{q})\, G\big(\mathbf{x}(\mathbf{p}) - \mathbf{x}(\mathbf{q})\big)\, \mathrm{d}S(\mathbf{q})\,, \tag{8.35}$$

where

$$\begin{aligned}\boldsymbol{\omega}\,(\mathbf{p}) &= \boldsymbol{\Gamma}\,(\mathbf{p})\,\delta(n) \\ &= \frac{1}{\left|\mathbf{t}_1 \times \mathbf{t}_2\right|}\left(\frac{\partial \mu}{\partial p_1}\mathbf{t}_2 - \frac{\partial \mu}{\partial p_2}\mathbf{t}_1\right)\delta(n).\end{aligned} \tag{8.36}$$

Equation (8.35) is a formal solution to Eq. (8.5) where $\boldsymbol{\omega}$ is a vorticity distribution. It is a delta distribution on the interface and its direction lies in the tangent plane. The quantity $\boldsymbol{\Gamma}$ is called the vortex sheet strength and it measures the jump in tangential velocity across the interface. The creation of the dipole strength Eq. (8.32) when $A \neq 0$ or $T \neq 0$ corresponds directly to the creation of a vortex sheet at the interface where the density jumps in value and/or when surface tension effects are present. While it is not easy to derive the equation for the generation of the vortex sheet strength from Eq. (8.4), it is relatively straightforward to derive an evolution equation for $\boldsymbol{\Gamma}$ from its definition in Eq. (8.36) and the evolution equation for the dipole strength Eq. (8.32), but the result is a complicated expression with no apparent advantage over the dipole formulation.

A specific feature of the particular formulation of free surface flow presented in this chapter is its generality since it allows fluids of different densities on either side of the interface. A similar approach[5] adopted to study water waves chooses the motion of the markers to be purely vertical,

which imposes some limitations on the geometry of the surface (breaking waves must be excluded). Both these approaches are the natural extension of the derivation in two-dimensions (one-dimensional surface)[6] which follows the pioneering work of Birkhoff.[7,8]

In contrast, most derivations of boundary integrals for free surface flow have picked one of the fluid densities to be zero, corresponding to one of the choices $A = \pm 1$. Bernoulli's equation Eq. (8.6) is used to update the potential on the free surface and various boundary integral techniques are used to solve Laplace's equation for the potential. The first derivation following this approach[9] uses a dipole representation in three dimensions, but only the application to axisymmetric flows is calculated numerically. Another technique,[10] developed first for two-dimensional flow,[11] uses Green's third identity to obtain a Fredholm integral equation of the first kind for the normal component of the velocity. Numerically, a full system of equations for the discrete approximation must be solved at each time level. In contrast, a Fredholm integral equation of the second kind for the normal component of the velocity given the potential along the interface[12] may be solved iteratively. It is also possible to prove numerical stability when a regularized Green's function is used in the numerical approximations, a technique developed first in two dimensions.[13] A different approach[14] uses a special surface parametrization to take advantage of the Riesz transform to ensure numerical stability of the boundary integral formulation based on dipole distributions. Finally, there are some special techniques, in particular those based on conformal mapping[15] or analytic continuation,[16,17] that can only be used in two-dimensional flows.

Perhaps the greatest strength of the formulation based on dipole distributions is that the integral equation Eq. (8.32) may be solved by modern iterative techniques, such as multigrid and GMRES with a suitable preconditioner. At each stage of the iteration, the cost in calculating the integral may be reduced with multipole or tree-code algorithms.[18,19] Moreover, the integrals for each $\mathbf{p}$ can be performed on separate processors leading to a natural procedure on parallel computer architectures. At the same time, the choice of α allows control on adaptivity. The physical choice $\alpha = A$ takes the density weighted average of the velocities at the interface as the interfacial velocity and proves to be an effective choice in many cases.

Assumptions so far include the presence of only a single interface, either closed or in open periodic geometry where the fluid is at rest far from the interface. If there is an additional external flow, it may be added directly in Eq. (8.18). There are other modifications and extensions for

the presence of multiple interfaces and the presence of solid boundaries. These modifications and extensions will be described later for the simpler case of two-dimensional flow. Indeed, a substantial amount of study has concentrated on two-dimensional flows both because of the simplification in the formulation and because of the much lower cost in computational time. It is appropriate, therefore, to state the formulation specifically for two-dimensional flow and describe the various modifications when additional free surfaces and rigid boundaries are present. The approach will be equally valid in three-dimensional flow.

8.2.2. *Two-dimensional BIT*

Introduce a right-handed coordinate system with unit vectors $\mathbf{i}, \mathbf{k}$ lying in the horizontal plane and $\mathbf{j}$ pointing vertically upwards. Gravity will be assumed to act vertically downwards. The flow is now assumed to lie in the $\mathbf{i}, \mathbf{j}$ only. A general parametric form for the interface location is

$$\mathbf{x} = x(p_1)\,\mathbf{i} + y(p_1)\,\mathbf{j} + p_2\,\mathbf{k}\,, \tag{8.37}$$

and the dipole distribution depends on $p_1 = p$ only,

$$\mu(\mathbf{p}) = \mu(p) \tag{8.38}$$

This choice ensures that the fluid velocity lies in the xy-plane only.

The tangent vectors Eq. (8.20)and the unit normal vector Eq. (8.23) are (with $p_1 = p$)

$$\mathbf{t}_1 = x_p\,\mathbf{i} + y_p\,\mathbf{j}\,, \quad \mathbf{t}_2 = \mathbf{k}\,, \quad \mathbf{n} = \frac{y_p}{s_p}\,\mathbf{i} - \frac{x_p}{s_p}\,\mathbf{j}\,, \tag{8.39}$$

where p is taken to run anti-clockwise (closed) or left to right (open), and

$$s_p^2 = x_p^2 + y_p^2 \tag{8.40}$$

gives the square of the derivative of the arclength: subscript p refers to differentiation.

The boundary integral Eq. (8.15) that determines the average potential at the interface becomes

$$I(p) = -\frac{1}{2\pi}\int \mu(q)\,\frac{y_q(q)\big(x(p)-x(q)\big) - x_q(q)\big(y(p)-y(q)\big)}{\big(x(p)-x(q)\big)^2 + \big(y(p)-y(q)\big)^2}\,\mathrm{d}q\,. \tag{8.41}$$

The vector potential has only one component $\mathbf{A} = \psi\,\mathbf{k}$; ψ is called the streamfunction. From Eq. (8.27), $A_1 = 0$ and $A_2 = \psi$, and from Eq. (8.24),

$$\psi(p) = \frac{1}{2\pi}\int \mu(q)\,\frac{x_q(q)\big(x(p)-x(q)\big) + y_q(q)\big(y(p)-y(q)\big)}{\big(x(p)-x(q)\big)^2 + \big(y(p)-y(q)\big)^2}\,\mathrm{d}q\,. \tag{8.42}$$

The velocity of the interface is determined by Eqs (8.28 and 8.29).

$$s_p^2 \mathbf{U} = \big(x_p\, I_p + y_p\, \psi_p\big)\, \mathbf{i} + \big(y_p\, I_p - x_p\, \psi_p\big)\, \mathbf{j}\,, \tag{8.43}$$

$$s_p^2 \mathbf{m} = x_p\, \mu_p\, \mathbf{i} + y_p\, \mu_p\, \mathbf{j}\,. \tag{8.44}$$

Let $\mathbf{U} = u\,\mathbf{i} + v\,\mathbf{j}$, then u, v are easily determined by Eq. (8.43) and the velocity components of the interface motion Eq. (8.16) are

$$\frac{\partial x}{\partial t} = u_I = u - \frac{\alpha}{2}\frac{\mu_p x_p}{s_p^2}\,, \tag{8.45}$$

$$\frac{\partial y}{\partial t} = v_I = v - \frac{\alpha}{2}\frac{\mu_p y_p}{s_p^2}\,. \tag{8.46}$$

The evolution of the dipole strength is determined by Eq. (8.32).

$$\frac{\partial \mu}{\partial t} - 2A\frac{\partial I}{\partial t} = -\frac{\alpha}{2}\frac{\mu_p^2}{s_p^2} - A\left[u^2 + v^2 - \alpha\,\frac{\big(u x_p + v y_p\big)\,\mu_p}{s_p^2} - \frac{1}{4}\frac{\mu_p^2}{s_p^2} - 2gy\right] - \frac{2T}{\rho_1 + \rho_2}\,\frac{x_p y_{pp} - y_p x_{pp}}{s_p^3}\,. \tag{8.47}$$

Unfortunately, the expression for the time derivative of I is lengthy, so it is convenient to introduce a more compact notation. Let $z(p) = x(p) + \mathrm{i}y(p)$ be the location of the interface in the complex plane. There is a natural connection between potential theory and complex variables and restatement of the formulation in terms of complex variables leads to other insights in the application of boundary integral methods to free surface flows in two dimensions.

Introduce the complex potential $\phi + \mathrm{i}\psi$. In particular, let the average complex potential at the interface be denoted $\Phi = I + \mathrm{i}\psi$. Then Eq. (8.41) and Eq. (8.42) may be combined into one complex integral,

$$\Phi(p) = \frac{1}{2\pi\mathrm{i}} \int \mu(q)\,\frac{z_q(q)}{z(q) - z(p)}\,\mathrm{d}q\,. \tag{8.48}$$

Of course, this integral must be taken in the principal-valued sense. It is clearly the parametric form of the Cauchy integral.

The complex velocity $w = u + \mathrm{i}v$ is related to the derivative of the complex potential. The average complex velocity Eq. (8.43) at the interface will be

$$w^*(p) = \frac{\Phi_p(p)}{z_p(p)}\,, \tag{8.49}$$

where the superscript $*$ refers to complex conjugation and the subscripts p indicate differentiation as before. The motion of the interface Eqs (8.45 and 8.46) becomes the complex weighted velocity

$$W^* = w^* - \frac{\alpha}{2}\,\frac{\mu_p}{z_p}\,, \tag{8.50}$$

$$\frac{\partial z}{\partial t} = W\,. \tag{8.51}$$

Equation (8.47) may be rewritten as

$$\frac{\partial \mu}{\partial t} - 2A\Re\biggl\{\frac{1}{2\pi \mathrm{i}}\int \frac{\partial \mu}{\partial t}(q)\,\frac{z_q(q)}{z(q)-z(p)}\,\mathrm{d}q\biggr\} = R(p) \tag{8.52}$$

where

$$\begin{aligned} R(p) = 2A\Re\biggl\{&\frac{1}{2\pi \mathrm{i}}\int \mu(q)\,\frac{W_q(q)}{z(q)-z(p)}\,\mathrm{d}q \\ &- \frac{1}{2\pi \mathrm{i}}\int \mu(q)\,\frac{z_q(q)\,\bigl(W(q)-W(p)\bigr)}{\bigl(z(q)-z(p)\bigr)^2}\,\mathrm{d}q\biggr\} + \left(\frac{A}{4}-\frac{\alpha}{2}\right)\frac{\mu_p^2}{s_p^2} \\ &- A\biggl[w^*w - \alpha\,\mu_p\,\Re\biggl\{\frac{w}{z_p}\biggr\} - 2g\Im\{z\}\biggr] - \frac{2T}{\rho_1+\rho_2}\,\frac{1}{s_p}\Im\biggl\{\frac{z_{pp}}{z_p}\biggr\}. \end{aligned} \tag{8.53}$$

Written this way, it is clear that Eq. (8.52) constitutes a Fredholm integral equation of the second kind for the rate of change of the dipole strength.

The connection between a dipole distribution and a vortex sheet representation is very easy to establish in this new notation. By integrating by parts, the complex velocity can be written as

$$\begin{aligned} w^* = \frac{\Phi_p}{z_p} &= -\frac{1}{2\pi \mathrm{i}}\int \mu(q)\,\frac{\mathrm{d}}{\mathrm{d}q}\left(\frac{1}{z(q)-z(p)}\right)\mathrm{d}q \\ &= \frac{1}{2\pi \mathrm{i}}\int \frac{\mu_q(q)}{z(q)-z(p)}\,\mathrm{d}q\,, \end{aligned} \tag{8.54}$$

which is the complex form for the Birkhoff-Rott integral that gives the motion of a vortex sheet. The vortex sheet strength is $\Gamma = \mu_p/s_p$; see Eq. (8.36). It is convenient, and common, to express μ_p as the unnormalized vortex sheet strength γ. The evolution equation for γ follows simply from differentiating Eq. (8.47) with respect to p. If there is no jump in density $A = 0$ and if surface tension may be neglected $T = 0$, the choice $\alpha = 0$ (the motion of the interface is the average velocity) means γ remains a constant in time. Thus,

$$\frac{\partial z^*}{\partial t} = \frac{1}{2\pi \mathrm{i}}\int \frac{\gamma(q)}{z(q)-z(p)}\,\mathrm{d}q \tag{8.55}$$

is the equation of motion for a vortex sheet, a well-studied equation as the model for a thin shear layer.[20,21]

There is an important difference between a dipole and vortex sheet representation. The mean value of the dipole strength is dynamically unimportant and the far-field motion is at rest. If the vortex sheet strength has a mean value then there is a net circulation in the region containing the interface and the far-field motion will reflect its presence. In particular, if the vortex sheet is in open, periodic geometry, then the fluids above and below the sheet flow past each other in a shearing motion. In this case, the mean value of γ is the jump in the velocities of the two fluids far from the sheet. In other words, if there is a mean shear flow at the interface, it is more appropriate to use a vortex sheet representation.

This completes the basic derivation of boundary integral methods for free surface flows. However, there is a useful modification for open, periodic geometries which is needed for studies of water waves and the Rayleigh-Taylor instability.

8.2.3. *Open, periodic geometry*

The Green's function, Eq. (8.11) or Eq. (8.12), used in the derivation of the boundary integrals for free surface flow is the free space Green's function. If there are geometrical constraints on the motion, there may be other Green's functions more appropriate for the boundary integrals. An obvious example is open, periodic geometry where the interface and its motion remain periodic in the horizontal plane. A periodic Green's function may be obtained by the method of images which then guarantees periodic motion.

For two-dimensional motion, the assumption will be that $z(p+L) = L + z(p)$ and $\mu(p+L) = \mu(p)$. Then

$$\begin{aligned}
\Phi(p) &= \frac{1}{2\pi \mathrm{i}} \int_{-\infty}^{\infty} \mu(q)\, \frac{z_q(q)}{z(q) - z(p)}\, \mathrm{d}q \\
&= \frac{1}{2\pi \mathrm{i}} \int_{0}^{L} \mu(q)\, z_q(q) \sum_{n=-\infty}^{\infty} \frac{1}{z(q) - z(p) - nL}\, \mathrm{d}q \\
&= \frac{1}{2L\mathrm{i}} \int_{0}^{L} \mu(q)\, z_q(q)\, \cot\left\{ \frac{\pi}{L} \big(z(q) - z(p) \big) \right\} \mathrm{d}q\,. \qquad (8.56)
\end{aligned}$$

The formula for the sum can be found in Reference 22. The standard choice is to scale z with $L/2\pi$ or equivalently set $L = 2\pi$. Besides the obvious replacement of the Green's function in the integrals in Eq. (8.52) and Eq. (8.53), the equations of motion for the interface remain unchanged.

The value of Eq. (8.56) is that the range of integration is finite, and the integrand is periodic allowing highly accurate spectral methods to be used numerically.

Unfortunately, the periodic Green's function in three dimensions requires a double sum that does not even converge. Fortunately, the sum can be modified so that it is convergent without destroying the nature of the Green's function; only the mean level of the Green's function is affected. Since only derivatives of the Green's function are needed in the boundary integrals, they remain unchanged. Even so, the modified sum has no known closed form and converges very slowly. Instead, the sum can be converted to rapidly converging Ewald sums.[9]

The boundary integral equations for free surface flow are nonlinear and only a few special solutions are known. A simple example is the perfectly flat interface which is stationary and the dipole strength is constant. Instead, the solutions to the equations must be constructed numerically. Section 8.3 will present the standard numerical methods for the case of open, periodic geometry.

8.2.4. *Linear stability analysis*

Before designing a numerical method, it is wise to have some understanding of the basic mathematical properties of the solution to the equations. A good starting point is to consider the stability of a flat interface with small perturbations. A linear analysis can establish the stability of the solutions and give insight into the general behavior of the interfacial motion. However, it is best to consider as general a case as possible, which means the inclusion of a mean value γ_0 to the vortex sheet strength to allow for a mean shearing motion.

Because the Lagrangian markers may move along the interface, the perturbations are written in the form,

$$z(p) = p + \frac{\alpha}{2}\gamma_0 t + a\mathrm{e}^{\mathrm{i}mp} + b\mathrm{e}^{-\mathrm{i}mp}\,, \tag{8.57}$$

$$\gamma(p) = \gamma_0 + c\mathrm{e}^{\mathrm{i}mp} + c^*\mathrm{e}^{-\mathrm{i}mp}\,, \tag{8.58}$$

where the coefficients a, b, c are assumed small. Note that the form of the perturbation in γ is designed to ensure that it is a real function: c^* is the complex conjugate of c. For convenience, only one mode m is selected. Once the results are known, a linear superposition of all integer modes will produce in effect a complete Fourier series allowing for arbitrarily small perturbations.

The evolution equations for the coefficients can be obtained by substituting Eqs (8.57 and 8.58) into Eqs (8.51 and 8.52), and retaining only those terms that are linear in the coefficients a, b, c;

$$\frac{\mathrm{d}a}{\mathrm{d}t} = -\frac{1+\alpha}{2}\left(c - \mathrm{i}m\gamma_0 b^*\right), \tag{8.59}$$

$$\frac{\mathrm{d}b^*}{\mathrm{d}t} = \frac{1-\alpha}{2}\left(c - \mathrm{i}m\gamma_0 a\right), \tag{8.60}$$

$$\frac{\mathrm{d}c}{\mathrm{d}t} = (A-\alpha)\mathrm{i}m\gamma_0 c + \frac{A-\alpha}{2}\gamma_0^2 m^2\left(a+b^*\right) + \Omega\left(a-b^*\right), \tag{8.61}$$

where

$$\Omega = Agm + \frac{Tm^3}{\rho_1+\rho_2}\,. \tag{8.62}$$

The general solution to this system of ordinary differential equations is

$$a = \varepsilon_1 + \varepsilon_2 a_+ \mathrm{e}^{\sigma_+ t} + \varepsilon_3 a_- \mathrm{e}^{\sigma_- t}, \tag{8.63}$$

$$b^* = \varepsilon_1 + \varepsilon_2 b^*_+ \mathrm{e}^{\sigma_+ t} + \varepsilon_3 b^*_- \mathrm{e}^{\sigma_- t}, \tag{8.64}$$

$$c = \varepsilon_1 \mathrm{i}m\gamma_0 + \varepsilon_2 c_+ \mathrm{e}^{\sigma_+ t} + \varepsilon_3 c_- \mathrm{e}^{\sigma_- t}, \tag{8.65}$$

where

$$\sigma_\pm = \frac{A-\alpha}{2}\mathrm{i}m\gamma_0 \pm \left(\frac{1-A^2}{4}\,\gamma_0^2 m^2 - \Omega\right)^{1/2}, \tag{8.66}$$

and

$$a_\pm = -\frac{1+\alpha}{2}\left(\sigma_\pm - \frac{1-\alpha}{2}\,\mathrm{i}m\gamma_0\right),$$

$$b^*_\pm = \frac{1-\alpha}{2}\left(\sigma_\pm + \frac{1+\alpha}{2}\,\mathrm{i}m\gamma_0\right),$$

$$c_\pm = \sigma_\pm^2 - \frac{1-\alpha^2}{4}\,\gamma_0^2 k^2\,.$$

The constants ε_j are determined by the initial conditions.

The constant ε_1 reflects a choice of initial condition in which the interface remains perfectly flat, while the Lagrangian markers are placed along the interface so that $\mu = \gamma_0 x$ remains unchanged. Normally, the choice of ε_1 is made to start with an initial concentration of Lagrangian markers where resolution is needed later in the calculation.

The more important behavior of the linear solution is the nature of the growth rates $\sigma_\pm$. Note first that the first term in Eq. (8.66) controls the tangential motion of the markers. It suggests that the choice $\alpha = A$ is

a natural one; this choice states that the average velocity at the interface should be weighted with the ratio of densities.

The physically relevant part of the behavior of the linear solution is determined by the term with the square root in Eq. (8.66). Consideration of a few special cases helps to shed light on the general case. First, consider $A = 1$. Physically, the density about the interface is negligible, as commonly assumed in the study of water waves, for example. Indeed,

$$\sigma_{\pm} = \pm \mathrm{i} \left(gm + \frac{Tm^3}{\rho_1} \right)^{1/2}, \tag{8.67}$$

which is just the standard dispersion relation for water waves.

Second, consider $A = -1$. Now the density below the interface is negligible and the surface is unstable (the Rayleigh-Taylor instability). The growth rates are

$$\sigma_{\pm} = \pm \left(gm - \frac{Tm^3}{\rho_2} \right)^{1/2}. \tag{8.68}$$

The instability is stabilized by surface tension for large wavenumbers.

The final choice is $A = 0$. There is no density difference across the interface as might occur for two immiscible fluids of equal density. If, in addition, $T = 0$, then the growth rates are

$$\sigma_{\pm} = \pm \frac{\gamma_0 m}{2}. \tag{8.69}$$

The motion is linearly ill-posed;[23] the modes with the smallest length scales (largest m) grow the fastest. This choice has received considerable attention for the last three decades since it describes the motion of a vortex sheet Eq. (8.55), the standard long wave model for a thin layer of vorticity. At first, hopes were that nonlinear effects would restore well-posedness, but these hopes have been dashed.[24,25] Indeed, there is strong evidence in Cowley et al. (and the references cited therein)[26] that vortex sheets develop curvature singularities in finite time. Surprisingly, the inclusion of surface tension effects, which stabilizes the highest modes according to linear theory, does not prevent singularity formation,[27] although the nature of the singularity has changed.

The above linear stability results have more applications than might be expected. By restricting attention to regions of an interface where it is locally flat and allowing the gravity vector to compensate for the orientation of the interface, it is possible to use the linear results to predict the stability under more general circumstances.[28] A good example is the late time

development of the Rayleigh-Taylor instability ($-1 < A < 0$) when heavier fluid falls in long spikes into the lower fluid. Along the sides of the spike, a local γ_0 grows slowly in time as the heavier fluid rushes by the lighter fluid and triggers the onset of a curvature singularity[29] and the subsequent roll up of the interface into a plume. In contrast, the case $0 < A < 1$ with no initial γ_0, does not appear to form a curvature singularity in finite time unless a breaking wave develops (a topological singularity of a different nature then occurs). Presumably, there are no regions where a mean vortex sheet strength arises for sufficient time to trigger curvature singularities. Singularity formation in interfacial flow remains an active area of research and is one of the remaining challenges for boundary integral methods.

For completeness and subsequent use, the linear results for the dipole strength are included when $\gamma_0 = 0$. Let

$$\mu(p) = d\mathrm{e}^{\mathrm{i}mp} + d^*\mathrm{e}^{-\mathrm{i}mp}\,. \tag{8.70}$$

Then the linear part of the potential Eq. (8.56) becomes

$$\begin{aligned}\Phi(p) &= \frac{1}{4\pi\mathrm{i}}\int_0^{2\pi}\left(d\mathrm{e}^{\mathrm{i}mq} + d^*\mathrm{e}^{-\mathrm{i}mq}\right)\cot\left(\frac{q-p}{2}\right)\mathrm{d}q \\ &= \frac{d}{2}\mathrm{e}^{\mathrm{i}mp} - \frac{d^*}{2}\mathrm{e}^{-\mathrm{i}mp}\,.\end{aligned} \tag{8.71}$$

The results Eqs. (8.63, 8.64 and 8.66) still stand, and $d_\pm = c_\pm/(\mathrm{i}m)$.

In summary, care must be taken in the design of numerical methods for interfacial flow because of the possibility of ill-posedness and subsequent formation of curvature singularities.

8.3. Numerical Approximation

The method of lines is a natural choice for the numerical treatment of the evolution of the interface. Markers along the interface are distributed in the Lagrangian variable p with an associated dipole strength. Then, the velocity and the rate of change of the dipole strength are calculated and used to update the marker's location and dipole strength through a standard method, such as the 4th-order Runge-Kutta method. Details will be provided here for free surface motion based on a dipole representation in open, 2π-periodic geometry, such as water waves. It is relatively straightforward to adapt the methods to other circumstances, such as the vortex sheet representation.

From now on, N markers are assumed to be evenly-spaced in p. Note that the definition of p is done in conjunction with the specification of the

initial conditions and can be done to improve resolution in the subsequent motion. Subsequent examples with water wave motion and the Rayleigh-Taylor instability will illustrate this idea. Let the location of the markers be $x_j = x(jh)$, $y_j = y(jh)$ with $h = 2\pi/N$. Similarly, let $\mu_j = \mu(jh)$. Since the interface is taken as 2π-periodic, the data may be expressed in terms of a discrete Fourier series. Let $f(p)$ stand for any 2π-periodic function in p (note that $x(p) - p$ is 2π-periodic). Then,

$$f_j = F_0^e + F_{N/2}^e(-1)^j + \sum_{m=1}^{N/2-1} \Big(F_m^e \cos(mjh) + F_m^o \sin(mjh) \Big) . \quad (8.72)$$

The odd/even Fourier coefficients F^o, F^e can be obtained through an application of the fast Fourier transform.

The first step in the numerical procedure is the calculation of the derivatives x_p, y_p and μ_p. Spectrally accurate results can be obtained by differentiating their Fourier series. The derivatives will be denoted as $(\mathcal{D}f)_j = f_p(jh)$, etc. Thus,

$$(\mathcal{D}f)_j = \sum_{m=1}^{N/2-1} mS(m) \Big(F_m^o \cos(mjh) - F_m^e \sin(mjh) \Big) . \quad (8.73)$$

Knowing the Fourier coefficients, the Fourier series in Eq. (8.72) can be evaluated through the fast Fourier transform. The inclusion of the factor $S(m)$ is to help suppress the ill-posed effects of differentiation. At the very least, it is important to suppress the effects of round-off errors by removing all Fourier coefficients that are close to machine precision. Otherwise, coefficients in the tail of the spectrum that might contain only round-off errors will be multiplied by a large m and exacerbate the effects of round-off in the derivatives.

The next step is the evaluation of Eq. (8.56). The difficulty in using a numerical approximation is that it is a principal-valued integral. Fortunately, the result

$$\frac{1}{4\pi \mathrm{i}} \int_0^{2\pi} z_q(q) \cot\left\{ \frac{z(q) - z(p)}{2} \right\} \mathrm{d}q = 0 \quad (8.74)$$

may be used to rewrite Eq. (8.56) without the pole singularity;

$$\Phi(p) = \frac{1}{4\pi \mathrm{i}} \int_0^{2\pi} \big(\mu(q) - \mu(p) \big) z_q(q) \cot\left\{ \frac{z(q) - z(p)}{2} \right\} \mathrm{d}q \, . \quad (8.75)$$

The integrand is now in a suitable form for the trapezoidal rule except for the indeterminate form when $q = p$. The limit is easily calculated, however,

and the approximation to the integral becomes

$$\Phi_j = \frac{1}{2N\mathrm{i}} \sum_{\substack{k\neq j \\ k=0}}^{N-1} \big(\mu_k - \mu_j\big)\,(\mathcal{D}z)_k\,\cot\!\left\{\frac{z_k - z_j}{2}\right\} + \frac{(\mathcal{D}\mu)_j}{N\mathrm{i}}\,. \tag{8.76}$$

It is also possible to apply the trapezoidal rule at alternate points that skip over the point $q = p$:

$$\Phi_j = \frac{1}{N\mathrm{i}} \sum_{\substack{k+j=\mathrm{odd} \\ k=0}}^{N-1} \big(\mu_k - \mu_j\big)\,(\mathcal{D}z)_k\,\cot\!\left\{\frac{z_k - z_j}{2}\right\}. \tag{8.77}$$

Both approximations are spectrally accurate, but Eq. (8.77) has a lower cost since only half the points are used. It also has the advantage that it is easier to programme on vector/parallel computers. It is still important to include the pole subtraction in Eq. (8.77) since it reduces the effects of round-off errors.

Another approach to the numerical treatment of the principal-valued integrals is to regularize the Green's function through convolution with a suitable smoothing function.[30] There are many possible choices for smoothing functions[31] and the specific choice does not seem to be crucial. A popular choice is the Krasny vortex blob method,[33] where

$$\cot\!\left\{\frac{z(q) - z(p)}{2}\right\} = \frac{\sin\big(x(q) - x(p)\big) - \mathrm{i}\sinh\big(y(q) - y(p)\big)}{\cosh\big(y(q) - y(p)\big) - \cos\big(x(q) - x(p)\big)} \tag{8.78}$$

is replaced by

$$\frac{\sin\big(x(q) - x(p)\big) - \mathrm{i}\sinh\big(y(q) - y(p)\big)}{\cosh\big(y(q) - y(p)\big) - \cos\big(x(q) - x(p)\big) + \delta^2}\,. \tag{8.79}$$

The integrand is no longer singular when $q = p$, and the pole singularity has been smoothed over a distance of $\mathcal{O}(\delta)$.

The original motivation for the regularization Eq. (8.79) was to ensure that vortex sheet motion ($A = \alpha = T = 0$) would exist globally in time. Indeed, appropriate regularizations[32] of the integrand guarantee solutions for all time and the limit of $\delta \to 0$ converges to a weak solution beyond the time of singularity formation. With $\delta > 0$, the vortex sheet rolls up into a spiral where the curvature singularity would otherwise form.[33] Only partial success is achieved when $-1 < A < 0$.[30] On the other hand, the regularized kernel does provide accurate simulations of water waves ($A = 1$) especially when δ is made proportional to s_p.[30] In other words, the blob size adjusts to the spacing of the Lagrangian markers. Incidentally,

Eq. (8.78) or Eq. (8.79) can be evaluated quickly by computing $\cos(x_j)$, $\sin(x_j)$, $\cosh(y_j)$ and $\sinh(y_j)$ first and using the expansion formulas to compute these functions with arguments that contain a difference.

The next step is to use the results of the numerical integration of the boundary integrals to determine the interfacial velocities Eqs. (8.50 and 8.51) by simply evaluating $(\mathcal{D}\Phi)_j$ through Eq. (8.73). Alternatively, the velocity may be determined directly from Eq. (8.54).

The last step requires a solution to Eq. (8.52). The discrete form is

$$\frac{\mathrm{d}\mu_j}{\mathrm{d}t} - 2A\Re\left\{\frac{1}{2N\mathrm{i}}\sum_{\substack{k\neq j\\k=0}}^{N-1}\left(\frac{\mathrm{d}\mu_k}{\mathrm{d}t}-\frac{\mathrm{d}\mu_j}{\mathrm{d}t}\right)(\mathcal{D}z)_k\,\cot\left\{\frac{z_k-z_j}{2}\right\}\right.$$
$$\left.+\frac{1}{N\mathrm{i}}\left(\mathcal{D}\frac{\mathrm{d}\mu}{\mathrm{d}t}\right)_j\right\} = R_j\,. \quad (8.80)$$

Note that R_j contains two integrals (see Eq. (8.53)) and it is advisable to remove the pole singularity in these integrals at $q = p$ by replacing $\mu(q)$ with $\mu(q) - \mu(p)$. Further, if the trapezoidal rule is to be applied as in Eq. (8.76), then the limiting values of the indeterminate forms in these integrals must be included. They require additional derivatives, which can be determined as in Eq. (8.73). The inclusion is not needed if the alternate point trapezoidal rule Eq. (8.77) is used.

Equation (8.80) is a system of linear equations for the rate of change of the dipole strength at the Lagrangian points. There are two main ways this system can be solved: direct methods based on an LU-decomposition, or iterative methods. Which choice is preferable depends on several factors, but generally iterative methods have the most advantages. The simplest iterative procedure is:

$$\frac{\partial\mu_j}{\partial t}^{(\nu+1)} = 2A\Re\left\{\frac{1}{2N\mathrm{i}}\sum_{\substack{k\neq j\\k=0}}^{N-1}\left(\frac{\mathrm{d}\mu_k}{\mathrm{d}t}^{(\nu)}-\frac{\mathrm{d}\mu_j}{\mathrm{d}t}^{(\nu)}\right)(\mathcal{D}z)_k\right.$$
$$\left.\times\cot\left\{\frac{z_k-z_j}{2}\right\}+\frac{1}{N\mathrm{i}}\left(\mathcal{D}\frac{\mathrm{d}\mu}{\mathrm{d}t}\right)_j^{(\nu)}\right\}+R_j\,. \quad (8.81)$$

Convergence[6] of the iteration has been established for $|A| \leq 1$. More importantly, when the interface is nearly horizontal, as in the propagation of water waves, the rate of convergence is very large so that only a few iterations are needed for even very high accuracy.

Several refinements are available. Each iteration in Eq. (8.81) takes $\mathcal{O}(N^2)$ operations to evaluate all the sums. Multipole expansions and tree codes[19] can reduce the count to $\mathcal{O}\big(N\log_2(N)\big)$ but with large setup costs so that N must be much larger than about 1,000 before significant savings are realized. Since the eigenvalue structure of the iteration is much like the typical structure of iteration operators for elliptic problems, multigrid strategies can be useful in reducing the effective number of iterations to just a few, and obviously the two methods can be combined. Finally, the first guess for the iterative solution can be improved since the dipole strength is evolving in time. For example, if a fourth-order predictor-corrector routine is used, it is simple to approximate the rate of change of the dipole strength by a cubic over the last four time steps and extrapolate (predict) the new value as the first guess for the iteration. Significant speed-up can be obtained this way.[6]

8.3.1. *Numerical stability*

Numerical stability is difficult to establish in general because of the differing nature of the solutions with different choices of A. But it is possible to conduct a linear stability analysis along the lines of Section 8.2.4. The difference is that the analysis depends on the specifics of the numerical approximation. It is advisable to break up the analysis into different parts to assess their influence on the stability. The starting point is to write

$$z_j = jh + \hat{z}_j\,, \quad \mu_j = \hat{\mu}_j\,, \tag{8.82}$$

where quantities with 'hats' will be assumed small. The linear version of Eq. (8.76) is

$$\Phi_j = \frac{1}{2N\mathrm{i}}\sum_{\substack{k\neq j\\ k=0}}^{N-1}\big(\hat{\mu}_k - \hat{\mu}_j\big)\,\cot\!\left\{\frac{kh-jh}{2}\right\} + \frac{(\mathcal{D}\hat{\mu})_j}{N\mathrm{i}}\,. \tag{8.83}$$

In line with Eq. (8.70), assume

$$\hat{\mu}_j = d\,\mathrm{e}^{\mathrm{i}mjh} + d^*\,\mathrm{e}^{-\mathrm{i}mjh}\,. \tag{8.84}$$

Equation (8.83) may be evaluated exactly by using the sum[34]

$$\frac{1}{2N\mathrm{i}}\sum_{\substack{k\neq j\\ k=0}}^{N-1}\mathrm{e}^{\pm\mathrm{i}mkh}\,\cot\!\left\{\frac{kh-jh}{2}\right\} = \pm\frac{1}{2}\mathrm{e}^{\pm\mathrm{i}mjh}\left(1-\frac{mh}{\pi}\right), \tag{8.85}$$

valid for $0 < mh \leq \pi$, to obtain

$$\Phi_j = \frac{d}{2}\,\mathrm{e}^{\mathrm{i}mjh}R(m) - \frac{d^*}{2}\,\mathrm{e}^{-\mathrm{i}mjh}R(m)\,, \tag{8.86}$$

where

$$R(m) = 1 + \frac{mh}{\pi}\left(S(m) - 1\right).$$

The presence of $S(m)$ in $R(m)$ arises from the contribution from $D\hat{\mu}_j$. By comparison with Eq. (8.71), $R(m) - 1$ is a measure of the relative error. For most spectral filters, $S(m) = 1$ for small m, and the approximation is exact. For mh near π, $S(m) \approx 0$, and the relative error is approximately 1. The error arises because the derivative of the high modes has been damped with $S(m)$ and the correction no longer balances the presence of μ_j in the sum. A simple remedy is to take the Fourier transform of μ_j, apply the filter $S(m)$ to the amplitudes and reconstitute a filtered version of μ to use in the sum. The result is that $R(m) = S(m)$; the potential has been effectively filtered. Remember to adopt the same procedure for the numerical approximation to the second and third integrals in Eq. (8.53).

The error for the alternate point quadrature Eq. (8.77) can be calculated in the same way by using the sum,

$$\frac{1}{N\mathrm{i}}\sum_{\substack{k+j=\mathrm{odd}\\ k=0}}^{N-1} \mathrm{e}^{\pm\mathrm{i}mkh}\,\cot\left\{\frac{kh-jh}{2}\right\} = \begin{cases} \pm\frac{1}{2}\mathrm{e}^{\pm\mathrm{i}mjh}\,, & 0 < mh < \pi\,,\\ 0\,, & mh = 0, \pi\,, \end{cases} \tag{8.87}$$

to obtain Eq. (8.86) except that $R(m) = 1$ for $0 < mh < \pi$, and $R(m) = 0$ for $mh = 0, \pi$. In other words, alternate point quadrature gives the exact results except for the Nyquist freguency $m = N/2$.

The rest of the analysis is straightforward and, with the appropriate expression for $R(m)$ depending on the choice of quadrature, leads to

$$\frac{\mathrm{d}a}{\mathrm{d}t} = -\frac{R(m)+\alpha}{2}\,\mathrm{i}md\,, \tag{8.88}$$

$$\frac{\mathrm{d}b^*}{\mathrm{d}t} = \frac{R(m)-\alpha}{2}\,\mathrm{i}md\,, \tag{8.89}$$

$$\frac{\mathrm{d}d}{\mathrm{d}t} = \frac{\tilde{\Omega}}{\mathrm{i}m}\left(a - b^*\right), \tag{8.90}$$

where

$$\tilde{\Omega} = Agm + \frac{Tm^3}{\rho_1 + \rho_2} S(m)\,, \tag{8.91}$$

which is the numerical version of Eqs (8.59 – 8.62), except that $c = \mathrm{i}md$ since we are using the dipole formulation and $\gamma_0 = 0$. The key difference is that the dispersion relation Eq. (8.66) is replaced by

$$\tilde{\sigma}_\pm = \pm \mathrm{i}\sqrt{\tilde{\Omega}\, R(m)\, S(m)}\,. \tag{8.92}$$

This numerical dispersion relationship is very close to the exact relationship, the difference being only the influence of the Fourier filter $S(m)$. Note, in particular, that $m = N/2$ gives $\tilde{\sigma}_\pm = 0$, and this may lead to nonlinear resonances.[35] In most methods,[36] this "sawtooth" mode is problematic, and remedies include its suppression,[36] regularization of the integrals,[30] interpolation of additional integration points[34,37] and polynomial smoothing.[11] For $0 < A \leq 1$, the modes are purely oscillatory and a suitable time-stepping method must be used, especially if N is large (the problem becomes 'oscillatory stiff'). Provided the time step is chosen small enough, the standard Runge-Kutta method is appropriate. The fourth-order Adams-Moulton method has also been used.[6]

8.4. Applications with a Single Surface

Given the importance of water in human existence, it is not surprising that the free surface flow of water and air occupies a large body of scientific study. Some important examples include the nature of water waves, the Rayleigh-Taylor instability, rising bubbles and falling drops. The development of boundary integrals methods for free surface flow has led to improved understanding of these flows through direct numerical simulation and mathematical analysis. The following three canonical examples will serve to illustrate the power of boundary integral methods. There are many more applications but the list is too long to review.

8.4.1. *Waves on deep water*

A wave travelling to the right on the surface of water whose mean height is zero can be constructed from the results of the linear analysis Eqs. (8.63, 8.64 and 8.70). Specifically, $A = \alpha = 1$, and for waves with long wavelengths, $T = 0$. Set $\varepsilon_1 = \varepsilon_2 = 0$ and $\varepsilon_3 = \varepsilon/\sqrt{gm}$ where ε is real and gives

the amplitude of the wave. The linear analysis predicts the motion to be

$$z(p) = p - \varepsilon \sin\bigl(mp - \sqrt{gm}\, t\bigr) + \mathrm{i}\varepsilon \cos\bigl(mp - \sqrt{gm}\, t\bigr)\,, \tag{8.93}$$

$$\mu(p) = -2\varepsilon\sqrt{\frac{g}{m}}\, \sin\bigl(mp - \sqrt{gm}\, t\bigr)\,. \tag{8.94}$$

An initial condition for numerical simulation is easily obtained by setting $t = 0$. Tests with ε small provide a good way to check the code. For moderate values of ε, around $\varepsilon = 0.3$, the waves steepen and break into little spillers. Larger choices for ε demonstrate breaking plungers as illustrated in Fig. 8.1. The physical scales are set with the choice $g = m = 1$, and $\varepsilon = 0.5$. The numerical parameters are $N = 4,096$, a time step of 0.0002 in the standard 4th-order Runge-Kutta method, and

$$S(m) = \frac{1}{2}\left\{1 - \tanh\left[40\left(\frac{2m}{N} - \frac{1}{4}\right)\right]\right\}. \tag{8.95}$$

This filter suppresses the top half of the discrete Fourier spectrum, in essence de-aliasing the spectral method and ensuring stability. The integral equation is solved by iteration until the iterates don't change by more than 10^{-10}.

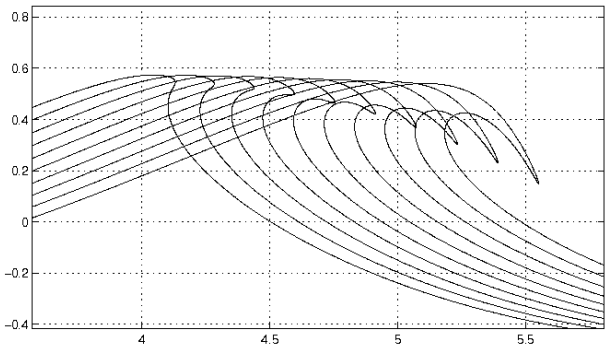

Fig. 8.1. Profiles of a plunging breaker at times staring at t=3.0 and increasing by 0.1 until t=4.0

What is striking about the results is the very high curvature at the tip of the plunging breaker. It reaches a value of 3.7×10^3. This level of accuracy is almost impossible to reach with other methods and highlights the impressive advantages that boundary integral methods can exhibit. It is also possible to confirm that the very large curvature is associated with a square

root singularity in the complex p-plane.[17] The singularity approaches the real axis of p but does not seem to reach it in finite time.

The plunging tip of the breaker has strong similarities to the falling spike that occurs during the Rayleigh-Taylor instability. The classical Rayleigh-Taylor instability occurs when heavy fluid falls into a vacuum, $A = -1$, $\alpha = -1$. For a perturbation with a single mode, a pattern of falling spikes and rising bubbles[38] quickly emerges. The spikes fall freely under gravity and the bubbles rise with constant speed. Eventually, the tip of the spike will develop a curvature large enough for surface tension effects to become important.[39,40] Then a drop forms at the tip which will subsequently detach, but this process cannot be described by the current boundary integral formulation. The nature of the Rayleigh-Taylor instability for a fluid layer is discussed in Section 8.5 and provides a typical example of a falling spike.

8.4.2. *Rising bubbles*

When a circular bubble of air is released, it rises and deforms into the shape of a hemispherical cap. Under these circumstances, $A = \alpha = 1$. The mathematical nature of the underlying elliptic problem reveals a deficiency in the dipole representation of the interfacial motion. The elliptic problem is an exterior one where the solution in the far field must be specified either as a constant or a logarithmic variation. A constant has no dynamic significance and may be neglected if there is no fluid motion in the far field. On the other hand, if the bubble expands as it rises, then there must be a net outflow of fluid in the far field to maintain conservation of mass. The outward flux F of fluid on the boundary of a large circle $r = R$ that encases the bubble at its centre will be

$$F = \int_0^{2\pi} \frac{\partial \phi}{\partial r}(R, \theta)\, R \mathrm{d}\theta \,. \tag{8.96}$$

Since the far-field behavior of a dipole is $1/|z|$, a dipole distribution cannot give the correct far-field behavior. Instead, a source term must be added to complete the representation of the potential; Eq. (8.48) is replaced with

$$\Phi_E(p) = \Phi + \frac{F(t)}{2\pi} \ln\big(z(p)\big) \,, \tag{8.97}$$

where F is real-valued. As a consequence, Eq. (8.49) must be replaced with

$$w^*(p) = \frac{\Phi_p(p)}{z_p(p)} + \frac{F}{2\pi z(p)} \,. \tag{8.98}$$

The only other changes that are necessary occur in Eq. (8.52). A term must be included to account for the difference between the pressure inside the bubble P_i and the pressure in the far-field P_o. Also, the change in outward flux must be included. As a consequence, Eq. (8.52) becomes (recalling that $A = \alpha = 1$, so $\rho_1 = \rho$ and $\rho_2 = 0$),

$$\frac{\partial \mu}{\partial t}(p) - 2\Re\left\{ \frac{1}{2\pi \mathrm{i}} \int \frac{\partial \mu}{\partial t}(q)\, \frac{z_q(q)}{z(q) - z(p)}\, \mathrm{d}q \right\} = R(p) + \frac{1}{\pi} \frac{\mathrm{d}F}{\mathrm{d}t}\, \ln|z(p)| + \frac{F}{\pi}\, \Re\left\{ \frac{w(p)}{z(p)} \right\} + 2\, \frac{P_o - P_i}{\rho}\,. \quad (8.99)$$

Setting aside for the moment that the rate of change of F is unknown, the integral equation for the rate of change of the dipole distribution is singular. A uniform rate of change of dipole distribution is a homogeneous solution to Eq. (8.99). Solutions to Eq. (8.99) exist only if the Fredholm alternative is satisfied.[41]

Let τ satisfy the homogeneous adjoint equation,

$$\tau(p) + 2\Re\left\{ \frac{z_p(p)}{2\pi \mathrm{i}} \int \frac{\tau(q)}{z(q) - z(p)}\, \mathrm{d}q \right\} = 0\,. \quad (8.100)$$

Then the application of the Fredholm alternative produces the relation

$$\frac{1}{2\pi} \frac{\mathrm{d}F}{\mathrm{d}t} \int \tau(p)\, \ln|z(p)|\, \mathrm{d}p = \int \left[\frac{P_i - P_o}{\rho} - R(p) \right] \tau(p)\, \mathrm{d}p - \frac{F}{2\pi} \int \Re\left\{ \frac{w(p)}{z(p)} \right\} \tau(p)\, \mathrm{d}p\,, \quad (8.101)$$

which provides an evolution equation for F. Equation (8.101) provides a clear connection between the outward flux and the pressure difference between the interior of the bubble and the far-field, modified by hydrodynamic and hydrostatic effects that appear in the other terms. There are several ways this connection can be exploited. For example, set $P_i = P_o$, and let the bubble rise under the influence of buoyancy effects. As the bubble rises, the hydrostatic pressure will lead to changes in $R(p)$, causing the bubble to expand ($F(t)$ will increase). The inside of the bubble may be regarded as a gas and P_i will change according to the equation of state as the volume of the bubble increases. All of these effects can be accommodated in Eq. (8.101).

Two examples of this formulation have been considered before. In one,[42] the initial rise and distortion of the bubble is simulated by both the dipole and vortex sheet methods for comparison purposes. Here, the expansion of

the bubble is neglected, so $F(t) = 0$ and P_i is allowed to adjust to satisfy Eq. (8.101) (not explicitly calculated). Equation (8.99) may still be solved by iteration as long as the undetermined homogeneous solution is specified. Since it is merely a uniform constant, it has no dynamic consequences. The iterations converge with the dipole held constant in time at the top of the bubble. An initially circular bubble of unit radius is released in the presence of a unit vertical gravity field. The rise and distortion of the bubble are shown in Fig. 8.2. The bottom of the bubble rises faster than the

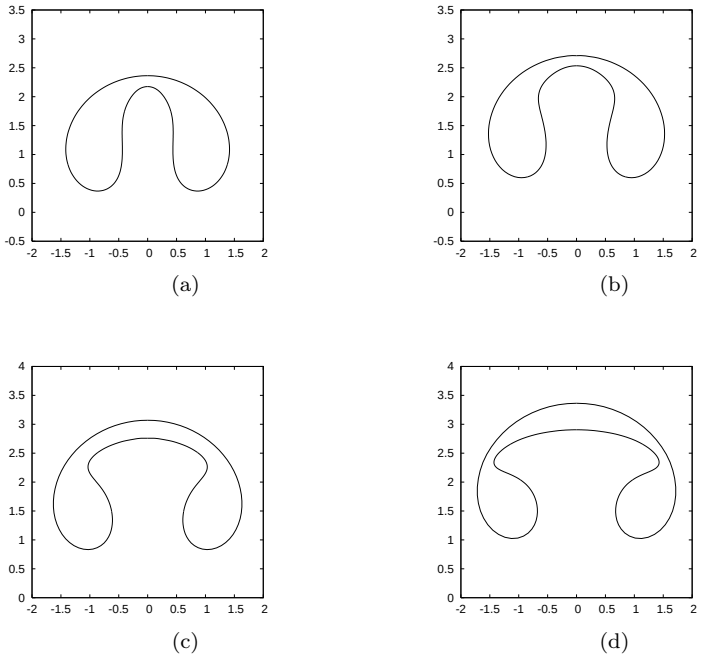

Fig. 8.2. Profiles of a rising bubble at times (a) $t = 2.5$, (b) $t = 3.0$ (c) $t = 3.5$ (d) $t = 4.0$.

top, forming an inward plume. The plume broadens and its sides approach the sides of the bubble. The appearance of the bubble is now that of a hemispherical cap with two attached lobes at its sides.

What is also noticeable in these results is the close approach of different parts of the surface to each other. Indeed, At $t = 4.0$ the code begins to fail as the neck of the two side lobes begin to pinch off. From the stand point of the numerical approximation, difficulties are arising because the

denominator in the integrand in Eq. (8.48) is becoming very small for values of q not close to p leading to large spikes in the integrand. This matter will be revisited as a future challenge in Section 8.6.

The other example where this formulation is used occurs when a high external pressure is used to attempt to collapse the bubble. Buoyancy is neglected because the outside pressure is large enough to force the bubble to collapse quickly not allowing the bubble enough time to rise. The inside pressure is allowed to increase according to the equation of state for gases, and it grows large enough to reverse the pressure gradient at a later time causing the surface to undergo Rayleigh-Taylor instability. For the numerical results presented in Ref. 9, the bubble is assumed axisymmetric but the derivation of the equations is essentially the same as the derivation for two-dimensional flow. In either case, Eq. (8.101) or its axisymmetric version must be used. See Reference 9 for further details.

8.5. Applications with Two Surfaces

In principle, the addition of more interfaces means simply the addition of more surface integrals. A good example is the study of triadic resonances between water waves and internal waves.[6] But there can be new features. The acceleration of thin liquid layers in gases requires modifications to the basic formulation similar to the formulation of external flow outside a single interface given in Sec. 8.4.

New considerations arise if one of the surfaces is a rigid boundary, as in shallow water or in the motion of a submerged body. Two specific examples will illustrate both of the necessary modifications.

8.5.1. *Rayleigh-Taylor instability of a liquid layer of finite thickness*

A liquid layer of density ρ lies between two horizontal surfaces with gas of negligible density above and below. If the surfaces are perfectly flat, then a pressure gradient $(P_1 - P_2)/(\rho g H)$ can hold the layer in place against the force of gravity. Here, P_1 and P_2 are the pressures below and above the layer respectively, and H is the mean thickness of the layer. This layer is unstable to perturbations, an example of the Rayleigh-Taylor instability. Also, the pressure difference may cause the layer to accelerate, a possibility that is allowed in the following description of the equations of motion.[43,44]

Let all quantities on the lower and upper surface be designated with

a subscript 1 and 2 respectively. From the assumed form of the layer, $A_1 = \alpha_1 = -1$ and $A_2 = \alpha_2 = 1$. The flow is assumed 2π-periodic and $\rho = g = 1$. The average complex potential at the surfaces induced by the dipole distributions is

$$\Phi_j(p) = \frac{1}{4\pi \mathrm{i}} \sum_{k=1}^{2} \int_0^{2\pi} \mu_k(q)\, z_{k,q}(q)\, \cot\left\{ \frac{z_k(q) - z_j(p)}{2} \right\} \mathrm{d}q\,. \tag{8.102}$$

Since the layer may move vertically with speed $V(t)$, a behavior not represented by dipole distributions, a term $-\mathrm{i}Vz_j$ must be added to Eq. (8.102). The complex velocity becomes

$$w_j^* = \frac{\Phi_{j,p}}{z_{j,p}} - \mathrm{i}V\,, \tag{8.103}$$

$$\frac{\partial z_j^*}{\partial t} = W_j^* = w_j^* - \alpha_j \frac{\mu_{j,p}}{z_{j,p}}\,. \tag{8.104}$$

The evolution equation for the dipole distributions are modifications of Eq. (8.52) as done in Eq. (8.99).

$$\frac{\partial \mu_j}{\partial t}(p) - 2A_j \sum_{k=1}^{2} \Re\left\{ \frac{1}{4\pi \mathrm{i}} \int_0^{2\pi} \frac{\partial \mu_k}{\partial t}(q)\, z_{k,q}(q) \cot\left\{ \frac{z_k(q) - z_j(p)}{2} \right\} \mathrm{d}q \right\}$$
$$= R_j(p) + 2A_j \frac{\mathrm{d}V}{\mathrm{d}t}\, y_j + 2A_j V v_j(p) + 2A_j \frac{P_j}{\rho}\,. \tag{8.105}$$

This coupled system of Fredholm integral equations of the second kind is singular and solutions exist provided the Fredholm alternative is satisfied.

$$\frac{\mathrm{d}V}{\mathrm{d}t} \sum_{j=1}^{2} A_j \int_0^{2\pi} y_j(p)\, \tau_j(p)\, \mathrm{d}p = -\sum_{j=1}^{2} A_j \int_0^{2\pi} \left[\frac{P_j}{\rho} + V v_j(p) \right] \tau_j(p)\, \mathrm{d}p$$
$$- \sum_{j=1}^{2} \int_0^{2\pi} R_j(p)\, \tau(p)\, \mathrm{d}p\,, \tag{8.106}$$

where τ_j is a nontrivial solution to the homogeneous adjoint equations,

$$\tau_j(p) + 2A_j \sum_{k=1}^{2} \Re\left\{ \frac{z_{k,p}(p)}{4\pi \mathrm{i}} \int_0^{2\pi} \tau_k(q)\, \cot\left\{ \frac{z_k(q) - z_j(p)}{2} \right\} \mathrm{d}q \right\} = 0\,. \tag{8.107}$$

The procedure to solve the adjoint equations numerically follow the methods already described in this chapter. Assume z_j and μ_j are known at some moment. They can be updated as follows. First, the integrals

in Eq. (8.102) are calculated by either Eq. (8.76) or Eq. (8.77) after applying the standard treatment for the principal-valued integrals. Second, the complex velocities are calculated, Eq. (8.103) and Eq. (8.104). Third, the eigenvector τ_j of the adjoint problem Eq. (8.107) is found by iteration. Fourth, the acceleration of the layer is calculated from Eq. (8.106) and finally the dipole equations Eq. (8.105) are solved by iteration. The iterative solution of the integral equations is made slightly complicated by the presence of two eigenvalues for the iteration matrix, one being $\lambda = 1$ which corresponds to the singular nature of the integral equations and another being $\lambda = -1$ which prevents convergence of the iteration. All other eigenvalues are less than 1 in magnitude. By shifting the eigenvalues and by specifying the unimportant homogeneous solutions to the dipole equations, the iterations can be made to converge.[41,43]

Results are shown in Fig. 8.3 for a layer located initially at

$$z_1(p) = P + \mathrm{i}\varepsilon\cos(P)\,,$$
$$z_2(p) = P + \mathrm{i}H\,,$$

with

$$P = p - \pi + \frac{1}{2}\sin(p)\,.$$

The mapping $P(p)$ is a good example of the way to cluster the Lagrangian points initially for good effect later in the calculation. They are concentrated in the region which will later become the rising bubble since the markers there are stretched apart as the bubble rises. The layer is assumed at rest initially, so $\mu_1 = \mu_2 = 0$. The fourth-order Adams-Bashforth-Moulton predictor-corrector is used with a time step of 0.005 and 128 markers. The layer, if perfectly flat, would be in hydrostatic balance, $P_1 = P_2 + \rho g H$. Physical scales are set with $\rho = g = 1$, $P_2 = 0$, $H = \pi/2$ and $\varepsilon = \pi/10$. Rather than drawing the location of the surfaces as curves passing through the Lagrangian markers, only the positions of the Lagrangian markers are shown in Fig. 8.3 to highlight the formation of numerical instability on the lower surface at late times.

The profiles in Fig. 8.3 show the drainage of fluid into falling spikes, while bubbles rise causing thin regions in the layer. Visible at $t = 3.0$ is the development of numerical instabilities on the lower surface at the top of the bubble. This is an example of the loss of accuracy when two different surfaces come close together causing the denominator $z_1(q) - z_2(p)$ in the integrals to become very small. This limitation prevents the numerical simulation from proceeding and being able to track this thinning region as

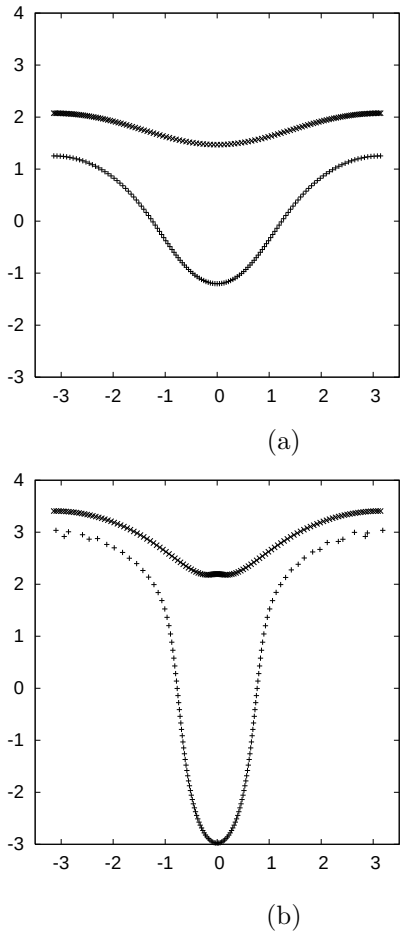

Fig. 8.3. Profiles of the layer at (a) $t = 2.0$, (b) $t = 3.0$.

it rises. This limitation is unfortunate since it prevents the calculations from establishing how quickly the region thins and eventually snaps apart under the influence of van der Waal forces.

8.5.2. *Water waves in finite depth*

There are many circumstances where fluid interfaces occur in the presence of rigid boundaries. A good example is the propagation of water waves over

bottom topography. Laplace's equation for the velocity potential Eq. (8.7) must now include a boundary condition at the rigid surface. Physically, the normal velocity of the fluid must match the normal velocity of the rigid surface. Let the rigid surface by represented in parametric form by $z_b(p)$ and its complex velocity $W_b(p)$. The downward normal velocity is

$$\frac{u_b y_{b,p} - v_b x_{b,p}}{s_{b,p}} = \Im\left\{ \frac{W_b^* z_{b,p}}{s_{b,p}} \right\} = \frac{\psi_{b,p}}{s_{b,p}} \,. \tag{8.108}$$

Even if the surface is moving, there is usually no flux through the surface. This implies that

$$\Im\left\{ \int W_b^* z_{b,p} \, \mathrm{d}p \right\} = \int \psi_{b,p} \, \mathrm{d}p = 0 \,. \tag{8.109}$$

Since there is no mean value to $\psi_{b,p}$, it has a Fourier series of the form Eq. (8.72), except that $F_0^e = 0$. The series may be integrated term-by-term and the result remains periodic. After integration, ψ_b has an arbitrary constant which may be taken as zero. Note in particular that if $W_b = 0$, the surface is stationary, and $\psi_b = 0$ is the obvious result.

Since ψ is the harmonic conjugate to ϕ, it too satisfies Laplace's equation. The Dirichlet boundary condition $\psi = \psi_b$ at the rigid surface can also be solved by a dipole distribution. For a 2π-periodic layer between a free surface $z_f(p)$ and the rigid boundary z_b, the complex potential may be written as

$$\begin{aligned} \phi + \mathrm{i}\psi = \frac{1}{4\pi\mathrm{i}} \int_0^{2\pi} \mu_f(q) \, z_{f,q}(q) \, \cot\left\{ \frac{z_f(q) - z}{2} \right\} \mathrm{d}q \\ + \frac{1}{4\pi} \int_0^{2\pi} \mu_b(q) \, z_{b,q}(q) \, \cot\left\{ \frac{z_b(q) - z}{2} \right\} \mathrm{d}q \,. \end{aligned} \tag{8.110}$$

The application of the boundary condition $\psi = \psi_b$ at $z = z_b$ leads to a Fredholm integral equation also of the second kind for μ_b.

$$\begin{aligned} \mu_b(p) + 2\Im\left\{ \frac{1}{4\pi\mathrm{i}} \int_0^{2\pi} \mu_f(q) \, z_{f,q}(q) \, \cot\left\{ \frac{z_f(q) - z_b(p)}{2} \right\} \mathrm{d}q \right. \\ \left. + \frac{1}{4\pi} \int_0^{2\pi} \mu_b(q) \, z_{b,q}(q) \, \cot\left\{ \frac{z_b(q) - z_b(p)}{2} \right\} \mathrm{d}q \right\} = \psi_b \,. \end{aligned} \tag{8.111}$$

As before, the second integral in Eq. (8.111) must be interpreted in the principal-valued sense. The evolution for μ_f follows the standard derivation for the dipole distribution at a free surface Eq. (8.52), except that the second integral in Eq. (8.110) must be included and leads to a time derivative of μ_b.

To complete the set of evolution equations, the time derivative of Eq. (8.111) must be included, leading to a set of coupled Fredholm integral equations of the second kind for the time derivatives of both dipole distributions.[6] These equations have been used to study water waves in shallow depth[6] and the downward acceleration of a rigid bottom that produces Rayleigh-Taylor instability on the falling free surface.[45]

A different application of this method calculates the motion of a rigid body beneath a water surface.[46] Here, the flow is not 2π-periodic. Instead, an infinite wave train is generated. A finite computational domain is chosen with damping layers attached to absorb the water waves as they leave the computational domain.

8.6. Some Challenges and Improvements

Spectral accuracy proves very desirable for tracking free surfaces in two-dimensional flow. The smooth calculation of the surface velocities prevents unwanted oscillations or instabilities from appearing during the motion. Unfortunately, in three-dimensional flow the accuracy of the numerical quadrature is limited, typically to third-order, and can result in numerical instability. Fortunately, there are accurate ways to treat axisymmetric geometry[47,48] through special properties of the elliptic functions which appear in the integrand. The hope is that there might be similar approaches for the full three-dimensional integrands.

Even for spectral methods in two-dimensional flow, significant accuracy is lost when two parts of the same surface or two different surfaces approach each other closely. Good examples are the pinch-off region in the rising bubble in Fig. 8.2 or the thinning region at the top of the rising bubble in Fig. 8.3. The culprit for the loss of accuracy is the rapid variation in the integrand which is nearly singular when the denominator in the integrand becomes small. To be specific, consider the integral,

$$I(p) = \frac{1}{2\pi \mathrm{i}} \int \frac{\mu_1(q)\, z_{1,q}(q)}{z_1(q) - z_2(p)}\, \mathrm{d}q\,. \tag{8.112}$$

When $z_1(q)$ is very close to $z_2(p)$, the denominator has large spikes of opposite sign on either side of the point of closest approach. Unless integration points are made available to resolve these spikes, large errors can arise in the numerical calculation of the integral.[41] One way to treat this difficulty is through interpolation by increasing the local resolution.[41] Another method uses the blob regularization and correction terms.[49]

A new method currently under development is the removal of the presence of the nearby pole singularity in the complex q plane of the integrand.[50] Seek the complex point Q such that $z_1(Q) = z_2(p)$. This means that Q is a function of p. Then rewrite

$$I(p) = \frac{1}{2\pi \mathrm{i}} \int \frac{\Big(\mu_1(q) - \mu_1(Q)\Big)\, z_{1,q}(q)}{z_1(q) - z_2(p)}\, \mathrm{d}q \pm \frac{\mu_1(Q)}{2}\,. \tag{8.113}$$

The sign of the additional term is determined by whether $z_1(q)$ lies below $z_2(p)$ $(+)$ or above $(-)$. Tests on a thin annulus reveal that spectral accuracy is restored more or less independently of the spacing between the surfaces. Unfortunately, the method relies on the ability to analytically continue both $z_1(q)$ and $\mu_1(q)$ into the complex q plane. Analytic continuation by means of the Fourier series is possible,[50] but other methods are currently being tested. Ultimately, the method must demonstrate success for free surface flows such as shown in Fig. 8.3.

There remain challenges for BITs when surfaces reconnect, for example when the tip of the plunging breaker shown in Fig. 8.1 reaches the surface below, or when the lobes of air pinch-off from the sides of the bubble in Fig. 8.2. There is no mathematical reason why these surfaces can't meet in finite time, but when they do, the boundary integral formulation becomes invalid. One might expect the surfaces to reconnect, but how? It is not just a matter of mathematics but also of physics since the processes by which reconnection occurs are not fully understood and probably occur on microscopic scales. There are methods, contour surgery in front tracking or level set methods which allow reconnection. There might be ways to use those techniques to design reconnection methods in boundary integral techniques.

Acknowledgments

I am indebted to two of my graduate students, Chao Xie and Jeong-Sook Im, for checking the results reported here. Chao Xie also provided me with the data for Fig. 8.1.

References

1. Pozrikidis C. (1992). *Boundary Integral and Singularity Methods for Linearized Viscous Flow*, Cambridge University Press, Cambridge.
2. Cottet G., Koumoutsakos P. (2000). *Vortex Methods*, Cambridge University Press, Cambridge.

3. Majda A., Bertozzi A. (2001). *Vorticity and Incompressible Flow*, Cambridge University Press, Cambridge.
4. Saffman P. (1992). *Vortex Dynamics*, Cambridge University Press, Cambridge.
5. Haroldsen D., Meiron D. (1998). Numerical calculation of three dimensional interfacial potential flows using the point vortex method. *SIAM J Sci Comp* 20: 648–683.
6. Baker G., Meiron D., Orszag S. (1982). Generalized vortex methods for free-surface flow problems. *J Fluid Mech* 123: 477–501.
7. Birkhoff G. (1954). *Los Alamos Sci. Lab. Report LA-1862*.
8. Birkhoff G. (1962). Helmholtz and Taylor instability. *Proc Symp Appl Maths Soc* 13: 55–76.
9. Baker G., Meiron D., Orszag S. (1984). Boundary integral methods for axisymmetric and three-dimensional Rayleigh-Taylor instability problems. *Physica D* 12: 19–31.
10. Broeze J., van Daalen E., Zandbergen P. (1993). A three-dimensional panel method for nonlinear free surface waves on vector computers. *Comput Mech* 13: 12–28.
11. Longuet-Higgins M., Cokelet E. (1976). The deformation of steep surface waves on water I. A numerical method of computation. *Proc Roy Soc Lond* A350: 1–26.
12. Beale J. (2001). A convergent boundary integral method for three-dimensional water waves. *Math Comp.* 70: 977–1029.
13. J. Beale, T. Hou and J. Lowengrub, Convergence of a boundary integral method for water waves, *SIAM J. Numer. Anal.* **33**, 1797–1843, (1996).
14. T. Hou and P. Zhang, Convergence of a boundary integral method for 3-D water waves, *Disc. Cont. Dynam. Sys.-Ser. B* **2**, 1–34, (2002).
15. R. Menikoff and C. Zemach, Rayleigh-Taylor instability and the use of conformal maps for ideal fluid flow, *J. Comput. Phys.* **51**, 28–64, (1983).
16. S. Tanveer, Singularities in water waves and Rayleigh-Taylor instability, *Proc. Roy. Soc. Lond.* **435**, 137–158, (1991).
17. S. Tanveer, Singularities in the classical Rayleigh-Taylor flow: formation and subsequent motion, *Proc. Roy. Soc. Lond.* **441**, 501–525, (1993).
18. J. Hamilton and G. Majda, On the Rokhlin-Greengard method with vortex blobs for problems posed in all space or periodic in one direction, *J. Comput. Phys.* **121**, 29, (1995).
19. K. Lindsay and R. Krasny, A particle method and adaptive treecode for vortex sheet motion in three-dimensional flow, *J. Comput. Phys.* **172**, 879–907, (2001).
20. D. Moore, The equations of motion of a vortex layer of small thickness, *Stud. Appl. Maths* **58**, 119, (1978).
21. M. Dhanak, Equation of motion of a diffusing vortex sheet, *J. Fluid Mech.* **269**, 265–281, (1994).
22. G. Carrier, M. Crook and C. Pearson, *Functions of a Complex Variable.* McGraw-Hill, New York (1966).
23. P. Saffman and G. Baker, Vortex Interactions, *Ann. Rev. Fluid Mech.* **11**, 95–122, (1979).

24. R. Caflisch and O. Orellana, Singular solutions and ill-posedness for the evolution of vortex sheets, *SIAM J. Math. Anal.* **20**, 293–307, (1989).
25. J. Duchon and O. Roberts, Global vortex-sheet solutions of Euler equations in the plane, *J. Diff. Equat.* **73**, 215–224, (1988).
26. S. Cowley, G. Baker and S. Tanveer, On the formation of Moore curvature singularities in vortex sheets, *J. Fluid Mech.* **378**, 233–267, (1999).
27. T. Hou, J. Lowengrub and M. Shelley, The long-time motion of a vortex sheets with surface tension, *Phys. Fluids* **9**, 1933–1954, (1997).
28. D. Joseph and T. Liao, Kelvin-Helmholtz mechanism for side branching in the displacement of light with heavy fluid under gravity, *Euro. J. Mech. B/Fluids* **11**, 253–264, (1992).
29. G. Baker, R. Caflisch and M. Siegel, Singularity formation during Rayleigh-Taylor instability, *J. Fluid Mech.* **252**, 51–78, (1993).
30. G. Baker and J. Beale, Vortex blob methods applied to interfacial motion, *J. Comput. Phys.* **196**, 233–258, (2003).
31. G. Baker and L. Pham, A comparison of blob methods for vortex sheet roll-up, *J. Fluid Mech.* **547**, 297–316, (2006)
32. J.-G. Liu and Z. Xin, Convergence of vortex methods for weak solutions to the 2D Euler equations with vortex sheet data, *Comm. Pure Appl. Maths* **48**, 611-628, (1995).
33. R. Krasny, Desingularization of periodic vortex sheet roll-up, *J. Comput. Phys.* **65**, 292, (1986).
34. G. Baker and A. Nachbin, Stable methods for vortex sheet motion in the presence of surface tension, *SIAM J. Sci. Comput.* **19**, 1737–1766, (1998).
35. D. Moore, A point vortex method applied to interfacial waves, in eds. H. Hornung and E.-A. Müller, *Vortex Motion*, Vieweg and Sohn, Braunschweig, Weisbaden, (1982).
36. J. Beale, T. Hou and J. Lowengrub, On the well-posedness of two fluid interfacial flows with surface tension, in eds. R. Caflisch and G. Papanicolaou, *NATO Adv. Sci. Inst. Ser. A*, 11–38, (1993).
37. A. Roberts, A stable and accurate numerical method to calculate the motion of a sharp interface between fluids, *IMA J. Appl. Math.* **31**, 13–35, (1983).
38. G. Baker, D. Meiron and S. Orszag, Vortex simulations of the Rayleigh-Taylor instability, *Phys. Fluids* **23**, 1485–1490, (1980).
39. D. Pullin, Numerical studies of surface-tension effects in nonlinear Kelvin-Helmholtz and Rayleigh-Taylor instabilities, *J. Fluid Mech.* **119**, 507–532, (1982).
40. Y. Yang, The initial value problem of a rising bubble in a two-dimensional vertical channel, *Phys. Fluids A*, **4**, 913–920, (1992).
41. G. Baker and M. Shelley, Boundary integral techniques for multi-connected domains, *J. Comput. Phys.* **64**, 112–132, (1986).
42. G. Baker and D. Moore, The rise and distortion of a two-dimensional gas bubble in an inviscid liquid, *Phys. Fluids A* **1**, 1451–1459, (1989).
43. G. Baker, R. McCrory, C. Verdon ans S. Orszag, Rayleigh-Taylor instability of fluid layers, *J. Fluid Mech.* **178**, 161-175, (1987).
44. G. Baker and Q. Nie, The asymptotic motion of an accelerating, thick layer

of inviscid liquid, *Phys. Fluids* **10**, 101-112, (1998).
45. G. Baker, The asymptotic motion of a tall column of liquid in a tube, in *Proc. 22nd Symp. Numer. Math.*, SANUM, Cape Town, RSA, (1998).
46. G. Baker, D. Meiron and S. Orszag, Generalized vortex methods for free surface flow problems II: Radiating waves, *J. Sci. Computing* **4**, 237, (1990).
47. M. Nitsche, Axisymmetric vortex sheet motion: Accurate evaluation of the principal-value integral, *SIAM J. Sci. Computing* **21**, 1066–1084, (1999).
48. Q. Nie, The nonlinear evolution of vortex sheets with surface tension in axisymmetric flows, *J. Comput. Phys.* **174**, 438–459, (2001).
49. J. Beale and M.-C. Lai, A method for computing nearly singular integrals, *SIAM J. Numer. Anal.* **38**, 1902–1925, (2001).
50. G. Baker and N. Golubeva, Improved accuracy for points near a surface in BIT, in eds. V. Minutolo, M. Aliabadi, *Advances in Boundary Element Techniques VIII*, ECLtd, UK, (2007). .